



HAL
open science

Microporomechanical behaviour of perfectly straight unidirectional fiber assembly : theoretical and experimental

Thang Tran, Christophe Binetruy, Sébastien Comas-Cardona, Nor-Edine Abriak

► **To cite this version:**

Thang Tran, Christophe Binetruy, Sébastien Comas-Cardona, Nor-Edine Abriak. Microporomechanical behaviour of perfectly straight unidirectional fiber assembly : theoretical and experimental. Composites Science and Technology, 2009, 69 (2), pp.199-206. 10.1016/j.compscitech.2008.10.015 . hal-01007044

HAL Id: hal-01007044

<https://hal.science/hal-01007044v1>

Submitted on 27 May 2024

HAL is a multi-disciplinary open access archive for the deposit and dissemination of scientific research documents, whether they are published or not. The documents may come from teaching and research institutions in France or abroad, or from public or private research centers.

L'archive ouverte pluridisciplinaire **HAL**, est destinée au dépôt et à la diffusion de documents scientifiques de niveau recherche, publiés ou non, émanant des établissements d'enseignement et de recherche français ou étrangers, des laboratoires publics ou privés.



Distributed under a Creative Commons Attribution - NonCommercial - NoDerivatives 4.0 International License

Microporomechanical behavior of perfectly straight unidirectional fiber assembly: Theoretical and experimental

Thang Tran^{a,b,*}, Christophe Binetruy^a, Sébastien Comas-Cardona^a, Nor-Edine Abriak^b

^aÉcole des Mines de Douai, Polymers and Composites Technology and Mechanical Engineering Department, 941 rue Charles Bourseul, BP 10838, 59508 Douai Cedex, France

^bÉcole des Mines de Douai, Civil and Environmental Engineering Department, 941 rue Charles Bourseul, BP 10838, 59508 Douai Cedex, France

The theory of poromechanics, most often used for macroscopically isotropic granular material, is applied to unidirectional fiber assemblies. When the deformation of the constituting fibers of those assemblies is taken into account during undrained forced compression, the Biot coefficients are expected to be lower than one. In the case of transversely isotropic materials, two independent Biot coefficients exist, one according to the fiber length direction and another relative to the plane perpendicular to that direction. The present paper aims at predicting the Biot coefficients for perfectly straight unidirectional (UD) fiber assemblies using micromechanical methods: dilute, Mori–Tanaka and Ponte Castañeda–Willis estimates. An experimental procedure, based on both uniaxial and triaxial material testing machines, is also detailed and applied to rubber fiber assemblies. The theoretical and experimental Biot coefficient results are compared and show a good agreement.

1. Introduction

Continuous fiber-reinforced composites have become increasingly accepted due to novel low-cost and high quality manufacturing process technologies. In the same time, natural fibers are emerging as low-cost, lightweight and environmentally superior alternatives to traditional reinforcing fibers and especially glass fibers in most applications using composites. Natural fibers-reinforced composites can be manufactured with existing technologies and compete with low to medium performance traditional composites. Weight reduction up to 30% compared to glass fiber-reinforced composites is achievable, for instance. Also, they exhibit good acoustical and thermal properties, are easier to trim and recycle (biodegradability of natural fibers), and are less abrasive compared to glass fiber-reinforced polymers. Finally, they can be associated to bio-based polymers to obtain green-composites.

Polymer composites are based on either thermoplastics or thermosetting resins. Processing such composites relies on various techniques, such as autoclave processing or compression molding, and involves either the compression of pre-impregnated fiber rein-

forcements or the flow of a viscous liquid within fibrous materials. The pressures involved during such processes can reach high levels due to:

- the compaction of the fibers getting closer to each other to attain the fiber volume fraction requirement;
- the fibrous media permeability drop because of the fiber volume fraction rise.

As a matter of fact, for some composite applications, the fiber volume fraction target often varies between 50% up to 70%. The liquid pressure involved during compression molding, for instance, can easily reach 2 or 3 MPa.

The lower mechanical performances and microstructure [3] of vegetal fibers compared to traditional synthetic fibers raise the question of the effect of such molding pressures on the structural integrity of the fibers [19]. Therefore, the application of vegetal fibers as reinforcements in composite materials requires a deeper investigation of the mechanical behavior of an impregnated fiber bed. First and for clarity, this article presents the analogy between soils and fiber-reinforced composites, the two similar porous media, and the terminology that is used hereafter. Next, after giving theoretical results of poroelasticity in granular mechanics and microporomechanics, theoretical solutions for densely packed unidirectional fiber assemblies are proposed. Then, tests on rubber fiber assembly samples are performed to determine the Biot

* Corresponding author. Address: École des Mines de Douai, Polymers and Composites Technology and Mechanical Engineering Department, 941 rue Charles Bourseul, BP 10838, 59508 Douai Cedex, France. Tel.: +33 (0)3 27 71 24 27; fax: +33 (0)3 27 71 29 81.

E-mail address: thang.tran@ensm-douai.fr (T. Tran).

coefficients. Finally, results from both theoretical and experimental sides are compared and discussed.

Fig. 1 shows the overall structure of this paper and the parameters to calculate theoretical and experimental Biot coefficients.

2. Granular and fibrous media

Granular and impregnated fibrous media can exhibit strong similarities in terms of constitution. It is well established in poromechanics [6], that a granular porous medium is constituted of a skeleton and an interstitial fluid (Fig. 2). The skeleton is composed of a matrix and a connected porosity. The matrix is made of solid grains, which can have occluded porosity. A fibrous medium, as shown in Fig. 2, consists of a fibrous reinforcement and a resin, which is in the liquid state during the early composite processing stage. The solid phase (fibrous reinforcement) is composed of fibers and connected porosity.

It should be noted that “matrix” is also often used and refers to a cured (polymerized) resin in a composite material. Therefore, to avoid any confusion, “matrix” will be used by mean of the composite terminology. Because the context of the article is composite manufacturing, the resin (which is in the liquid state) will be exclusively named either liquid or fluid.

In the following, bold-faced letters refer to second-order tensors, open-font letters refer to fourth-order tensors and the colon (: operator represents the double contracted product on two indices.

3. Impregnated porous media

3.1. Background

In previous composite manufacturing studies, where compression of impregnated fibrous media is involved [12,13,20], researchers have been using Terzaghi’s equation. This soil mechanics result (Eq. (1)) relates the total stress tensor Σ of an impregnated porous media as the function of the stress tensor applying on the porous skeleton Σ' and the interstitial liquid pressure P

$$\Sigma = \Sigma' - \delta P \quad (1)$$

where δ is the second-order unit tensor

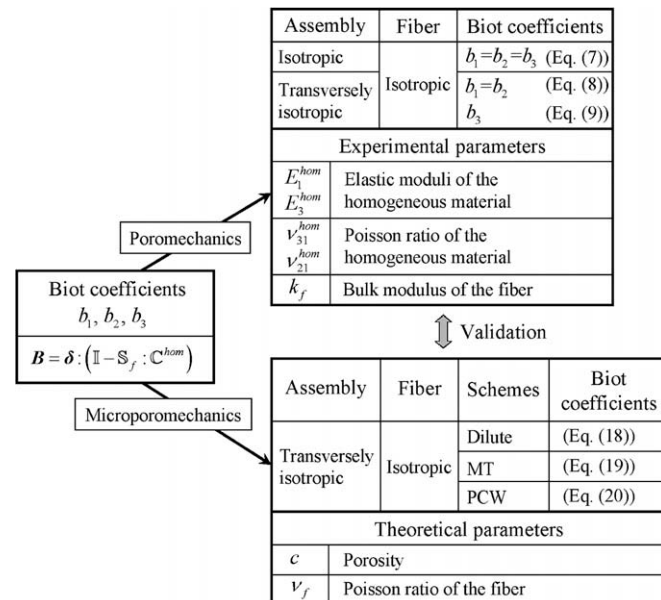


Fig. 1. Overall structure and main parameters of this paper.






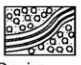


	Granular	Fibrous
Solid constituents	 Solid grain Occluded porosity } \Rightarrow Matrix	 Fiber (no occluded porosity)
Solid phase	 Matrix Connected porosity } \Rightarrow Skeleton	 Fiber Connected porosity } \Rightarrow Fibrous reinforcement
Liquid phase	 Interstitial fluid	 Resin
Porous medium	 Skeleton Interstitial fluid } \Rightarrow Granular porous medium	 Fibrous reinforcement Resin } \Rightarrow Fibrous porous medium

Fig. 2. Analogy between porous granular media and fibrous media.

$$\delta_{ij} = 1 \text{ if } i = j; \quad \delta_{ij} = 0 \text{ if } i \neq j \quad (2)$$

When the constituents deform due to their own compressibility under hydrostatic pressure, it is necessary to introduce the second-order Biot tensor \mathbf{B} in Terzaghi’s relationship

$$\Sigma = \Sigma' - \mathbf{B}P \quad (3)$$

The Biot tensor components are positive, inferior to one and for anisotropic materials, \mathbf{B} is diagonal [6]

$$\mathbf{B} = \begin{pmatrix} b_1 & 0 & 0 \\ 0 & b_2 & 0 \\ 0 & 0 & b_3 \end{pmatrix} \quad (4)$$

b_1 , b_2 and b_3 are the three components of the Biot tensor in the three respective cartesian coordinates.

For most soils, the grains are supposed infinitely rigid compared to the material they form, thus the Biot tensor reduces to the second-order unit tensor (Terzaghi’s hypothesis). For isotropic material, the three components of the Biot tensor are identical. For transversely isotropic or tetragonal materials, there are two different components and for the orthotropic or anisotropic material, the three components of the Biot tensor are distinct.

Using results from poroelasticity, the Biot tensor can be expressed as function of the fourth-order drained homogeneous elastic tensor \mathbb{C}^{hom} (stiffness tensor) of the skeleton and of the fourth-order elastic compliance tensor \mathbb{S}_f of the constituent [7]

$$\mathbf{B} = \delta : (\mathbb{I} - \mathbb{S}_f : \mathbb{C}^{hom}) \quad (5)$$

where \mathbb{I} is the fourth-order unit tensor

$$I_{ijkl} = \frac{1}{2} (\delta_{ik}\delta_{jl} + \delta_{il}\delta_{jk}) \quad (6)$$

The main work for the calculation of the Biot tensor consists in the calculation of the \mathbb{C}^{hom} tensor.

3.2. Application to fiber assemblies

The composite manufacturing issues present analogies with the ones studied in soil mechanics where relations have been established within the framework of the theory of the poroelasticity. Although the deformation of the fibrous material in the processing polymer composites is finite and not linear (region a in Fig. 3),

infinitesimal strains and linear behaviors are first applied in this work for the perfectly straight unidirectional fiber material (region b). This region corresponds to a high compression force.

For fiber assemblies, the Biot tensor's components can be considered within two particular cases of symmetry:

- both fiber assembly and individual fiber are isotropic (the case of glass mat, for example). In this case, $b_1 = b_2 = b_3 = b$, and the well-known relation (see, e.g. [6]) applies

$$b = 1 - \frac{k_{hom}}{k_f} \quad (7)$$

where k_{hom} and k_f are the bulk moduli of the homogeneous (fibrous) material and the individual fiber, respectively;

- the fiber assembly is transversely isotropic with an axis of revolution Ox_3 and the individual fiber is isotropic. The transverse isotropy is only due to the presence of inter-fiber aligned pores. In this case [10]

$$b_1 = b_2 = 1 + \frac{1 + \nu_{31}^{hom}}{3k_f \left(\frac{2(\nu_{31}^{hom})^2}{E_3^{hom}} - \frac{1 - \nu_{21}^{hom}}{E_1^{hom}} \right)} \quad (8)$$

$$b_3 = 1 + \frac{E_3^{hom} \left(\frac{2\nu_{31}^{hom}}{E_3^{hom}} + \frac{1 - \nu_{21}^{hom}}{E_1^{hom}} \right)}{3k_f \left(\frac{2(\nu_{31}^{hom})^2}{E_3^{hom}} - \frac{1 - \nu_{21}^{hom}}{E_1^{hom}} \right)} \quad (9)$$

where E_3^{hom} , E_1^{hom} , ν_{31}^{hom} and ν_{21}^{hom} are the elastic moduli and the Poisson ratios of the drained homogeneous material.

The relations of the Biot coefficients (Eqs. (8) and (9)) are calculated as a function of homogeneous moduli and Poisson ratios which are unknown, therefore specific tests will be performed so as to measure them (Section 5). In parallel, analytic relations of the Biot coefficients as a function of:

- the mechanical constants of the fiber (constituent)
- and porosity of the assembly

will be derived using micromechanical approaches. The fiber assembly has been modelled with the following assumptions (region b in Fig. 3):

- it is linear elastic;
- it consists of aligned, parallel, linear elastic and isotropic fibers;
- it is modelled with cylindrical pores.

The microporomechanical approaches with these assumptions are presented in the following section.

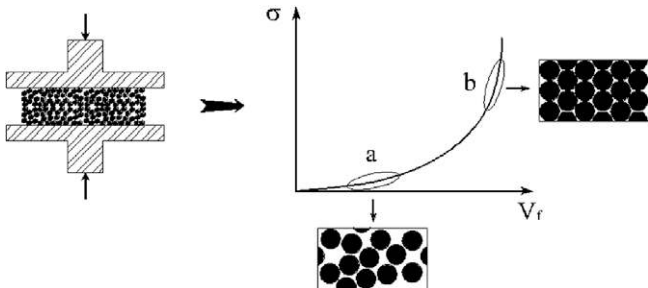


Fig. 3. Compression curve (stress σ –fiber volume fraction V_f) and the corresponding fiber structure.

4. Microporomechanical approach

4.1. Background

The stiffness tensor \mathbb{C}^{hom} can be determined by various micromechanical methods: bounds and estimated schemes. The Voigt and Reuss bounds cannot be applied for a transversely isotropic material (composed of isotropic constituents) because those bounds do not take into account the total anisotropy due to the arrangement of these constituents [4]. Regarding the bounds of Hashin–Shtrikman [18], only the upper bound exists. The lower one does not exist because it is obtained when the softest constituent is chosen like the reference material (in the case of a porous material, the softest constituent is the pore). Therefore in this present work, only estimated dilute, Mori–Tanaka [7] and Ponte Castañeda–Willis [18] schemes are studied. They are calculated based on the Eshelby tensor \mathbb{S}_E or Hill tensor \mathbb{P} which are determined analytically [9,16,21] with inhomogeneities of the ellipsoidal shape (three principal semi-axis a_1 , a_2 and a_3). The \mathbb{S}_E and \mathbb{P} tensors can be also calculated numerically for the general case of the ellipsoidal inhomogeneity with an arbitrary orientation [10,11]. The solutions of three above estimated schemes will be compared to choose the adapted schemes.

In this section, three schemes will be studied in order to increase the complexity of their respective modeling assumptions. The first one is the dilute scheme (also called the Eshelby scheme), which is used for low porosity (lower than 10%). Because of the low porosity in the material, the pores are supposed as non-interacting, the reference medium for the case of porous material is the individual fiber (Fig. 2). The formulation to calculate the homogeneous stiffness tensor \mathbb{C}_{dil}^{hom} according to this scheme writes (see, e.g. [7] or [8])

$$\mathbb{C}_{dil}^{hom} = \mathbb{C}_f + c(\mathbb{P} - \mathbb{S}_f)^{-1} \quad (10)$$

where c is the porosity; \mathbb{C}_f is the fourth-order stiffness tensor of the fiber; \mathbb{P} is the Hill tensor, $\mathbb{P} = \mathbb{S}_E : \mathbb{S}_f$, \mathbb{S}_E is the Eshelby tensor which depends on both the geometry of the inhomogeneity and the reference medium.

The dilute estimate is restricted to an infinitesimal porosity, in which the mechanical interaction between pores can be neglected, but \mathbb{C}_{dil}^{hom} obeys all properties of an elastic tensor [2].

To overcome the limitation of the dilute estimate and to account for the mechanical interaction between pores, the Mori–Tanaka estimate has been proposed. The porosity in the Mori–Tanaka scheme can reach up to 20% [4], the individual fiber is still considered as the reference medium. The homogenous stiffness tensor for the Mori–Tanaka scheme is (see, e.g. [7])

$$\mathbb{C}_{MT}^{hom} = (1 - c)\mathbb{C}_f : \left((1 - c)\mathbb{I} + c(\mathbb{I} - \mathbb{P} : \mathbb{C}_f)^{-1} \right)^{-1} \quad (11)$$

However, the non-diagonal symmetry, in some cases, of the homogeneous stiffness tensor \mathbb{C}_{MT}^{hom} may appear and is difficult to interpret [5].

The third scheme studied is the Ponte Castañeda–Willis estimate which, furthermore, takes into account the spatial distribution of the pores through a distribution function. The development of this scheme is based on the variational formulation of Hashin and Shtrikman, and the reference material is always taken identically to the individual fiber. For the case where all the pores have the same orientation, the homogeneous stiffness tensor of the Ponte Castañeda–Willis scheme writes (see, for more details [18])

$$\mathbb{C}_{PCW}^{hom} = \mathbb{C}_f + \left(\frac{1}{c} (\mathbb{P}_i - \mathbb{S}_f) - \mathbb{P}_d \right)^{-1} \quad (12)$$

Here \mathbb{P}_i is equivalent to \mathbb{P} in the two previous schemes (it characterizes the shape of the pores) while \mathbb{P}_d characterizes the spatial distribution of the pores in the material.

Contrarily to the Mori–Tanaka scheme, both pair and diagonal symmetries of the homogeneous stiffness tensor \mathbb{C}_{PCW}^{hom} are assured. However, a drawback of this scheme is the risk to have a difficulty to inverse tensors in Eq. (12) [4].

4.2. Application to unidirectional fiber assemblies

4.2.1. Homogenization schemes

To facilitate calculation with fourth-order tensors, the Walpole basis is used [4,22]. In this derivation, the notation of the Walpole basis is as in [22], thus the fourth-order unit tensor \mathbb{I} , the compliance \mathbb{S}_f and stiffness \mathbb{C}_f tensors of the matrix, and the three tensors \mathbb{P} , \mathbb{P}_i , \mathbb{P}_d writes

$$\mathbb{I} = \left\{ \begin{bmatrix} 1 & 0 \\ 0 & 1 \end{bmatrix}, 1, 1 \right\} \quad (13)$$

$$\mathbb{S}_f = \left\{ \begin{bmatrix} \frac{1}{E} & -\frac{\sqrt{2}\nu}{E} \\ -\frac{\sqrt{2}\nu}{E} & \frac{1-\nu}{E} \end{bmatrix}, \frac{1+\nu}{E}, \frac{1+\nu}{E} \right\} \quad (14)$$

$$\mathbb{C}_f = \left\{ \begin{bmatrix} \frac{1}{E} & -\frac{\sqrt{2}\nu}{E} \\ -\frac{\sqrt{2}\nu}{E} & \frac{1-\nu}{E} \end{bmatrix}^{-1}, \frac{E}{1+\nu}, \frac{E}{1+\nu} \right\} \quad (15)$$

$$\mathbb{P} = \mathbb{P}_i = \left\{ \begin{bmatrix} 0 & 0 \\ 0 & \frac{(1-2\nu)(1+\nu)}{2E(1-\nu)} \end{bmatrix}, \frac{(3-4\nu)(1+\nu)}{4E(1-\nu)}, \frac{1+\nu}{2E} \right\} \quad (16)$$

$$\mathbb{P}_d = \left\{ \begin{bmatrix} \frac{(1+\nu)(7-10\nu)}{15E(1-\nu)} & -\frac{\sqrt{2}(1+\nu)}{15E(1-\nu)} \\ -\frac{\sqrt{2}(1+\nu)}{15E(1-\nu)} & \frac{2(1+\nu)(3-5\nu)}{15E(1-\nu)} \end{bmatrix}, \frac{2(1+\nu)(4-5\nu)}{15E(1-\nu)}, \frac{2(1+\nu)(4-5\nu)}{15E(1-\nu)} \right\} \quad (17)$$

where E and ν are the Young modulus and the Poisson ratio of the isotropic individual fiber.

The ellipsoidal pores are considered cylindrical in all the three schemes (i.e., three semi-axis $a_1 = a_2$, $a_3 \rightarrow \infty \Rightarrow$ aspect ratio $\omega_i = \frac{a_3}{a_i} \rightarrow \infty$). The pores distribution in the Ponte Castañeda–Willis scheme is taking the circular form ($\omega_d = 1$) (see [18] for more details as well as the expression of ω_d).

The homogeneous stiffness tensors \mathbb{C}_{dil}^{hom} , \mathbb{C}_{MT}^{hom} and \mathbb{C}_{PCW}^{hom} of the three schemes are determined using Eqs. (10)–(12). The results obtained are then substituted in Eq. (5) to calculate the Biot tensor.

The calculations lead to the following results for the Biot coefficients for three schemes. In the case of the dilute scheme

$$b_1^{dil} = b_2^{dil} = \frac{2c(1-\nu)}{1-2\nu}; \quad b_3^{dil} = \frac{c}{1-2\nu} \quad (18)$$

For the Mori–Tanaka scheme, the Biot coefficients estimates are

$$b_1^{MT} = b_2^{MT} = \frac{2c(1-\nu)}{1-2\nu+c}; \quad b_3^{MT} = \frac{c[1+c(1-2\nu)]}{1-2\nu+c} \quad (19)$$

and for the Ponte Castañeda–Willis scheme, the Biot coefficients are

$$b_1^{PCW} = b_2^{PCW} = \frac{6c(1-\nu)[2c(4-5\nu)+15(1-\nu)]}{4c^2(1+\nu)(4-5\nu)+c(60\nu^2-99\nu+57)+45(1-\nu)(1-2\nu)} \quad (20)$$

$$b_3^{PCW} = \frac{3c(1-\nu)[4c(4-5\nu)+15]}{4c^2(1+\nu)(4-5\nu)+c(60\nu^2-99\nu+57)+45(1-\nu)(1-2\nu)}$$

The Biot coefficients of the transversely isotropic material, which has isotropic constituents, only depend on the porosity c and the Poisson ratio ν of the constitutive fiber. The modulus of the fiber cancels out during derivations.

4.2.2. Theoretical curves

The results of the Biot coefficients of the three schemes are presented in Fig. 4 with a Poisson ratio ν equal to 0.4. The curves for the dilute scheme are very different to other schemes because

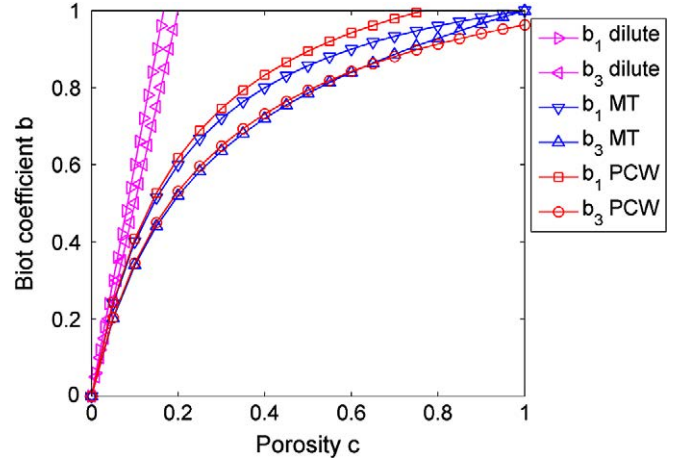


Fig. 4. Curves of the Biot coefficients for the three schemes, with $\nu = 0.4$.

the assumptions of this scheme are that the pores are unconnected and do not interact between each other. The Mori–Tanaka scheme is the only one which tends towards one when the porosity tends towards one, the Ponte Castañeda–Willis scheme for the circular distribution of the fiber is not much different to the Mori–Tanaka, except the fact that the Biot coefficients is only approximated to one when the porosity tends towards one.

With a value of ν approximated to 0.5, the curves of all schemes (except the dilute one) are quasi coincident. For the very low values of porosity, the three schemes give almost identical Biot coefficients. The value of b_1 is always greater than that of b_3 .

Because the Mori–Tanaka and Ponte Castañeda–Willis schemes are valid for a wider range of porosity, they will be compared to the experimental results, which are obtained with tests on unidirectional rubber fiber samples.

5. Tests on the rubber fiber samples

To verify the theoretical results and to obtain the Biot coefficients through experimentation for the transversely isotropic material, tests have been realized on the rubber fiber samples. The rubber material is chosen because its rigidity is low and therefore it reduces measurement errors during experiments, especially for the undrained isotropic compression test. The fibers are made of nitrile butadiene rubber whose Young modulus is 15 MPa and Poisson ratio is 0.48. Great care has to be taken during this test, because the values of isotropic deformation of the fibers are very small and in the same range of the effect of the compressibility of the confined water, the deformation of the cell... The measurement of Biot coefficients is not widespread, even for isotropic materials. For such cases, the reader may refer to the works of Bemer et al. [1] and Ozanam et al. [17], where the measured Biot coefficient of clay is found to be lower than one and to decrease when applied stress increases.

In the present work, the Biot coefficients are measured for the two arrangements of unidirectional rubber fibers: square and hexagonal (Fig. 5). The choice is limited to two arrangements because this paper focuses on the study of perfectly straight unidirectional fiber assembly of low porosity (region b in Fig. 3). The hexagonal fiber arrangement material is calculated such as a transversely isotropic material [14], thus the formulae to determine the Biot coefficients are Eqs. (8) and (9). For the square fiber arrangement material, the material symmetry is not transversely isotropic because the behaviors of the two perpendicular directions in the plane perpendicular to the fiber are not the same. This type of symmetry is called tetragonal and its homogeneous stiffness tensor has



Fig. 5. Square (left) and hexagonal (right) arrangements.

six separate components. The formulae to calculate the Biot coefficients of the transversely isotropic and of the tetragonal material as function of the homogeneous moduli are fortunately the same (Eqs. (8) and (9)), even though they have a different symmetry.

The calculation of the Biot coefficients (square and hexagonal fiber arrangements) require to measure five moduli: the bulk modulus of the fiber k_f ; the elastic moduli and the Poisson ratios of the drained homogeneous material E_3^{hom} , E_1^{hom} , ν_{31}^{hom} and ν_{21}^{hom} . It should be noted that the direction Ox_3 is always oriented along the axis of the fiber.

Because there are various moduli of different natures to be measured, different tests are performed (Table 1). The fiber bulk modulus k_f is measured by undrained isotropic compression test (triaxial machine). The homogeneous elastic moduli according to the direction 1 and 3 (E_1^{hom} and E_3^{hom}) are measured by unidirectional compression test (unidirectional compression machine) and shear test (triaxial machine). The measured results of the two tests are then compared and the best ones are chosen (compared to the Young modulus of the rubber). The Poisson ratio ν_{31}^{hom} is measured by shear test and ν_{21}^{hom} is determined via the drained homogeneous bulk modulus k^{hom} , k^{hom} is measured like k_f but in drained condition.

Sample geometry and test conditions are given in Table 2, the diameter of the rubber fibers is 5 mm. The detail of each test and the associated results are given in the following sections. For drained and undrained compression, the liquid is water.

5.1. Unidirectional compression tests

The square and hexagonal arrangement samples are tested with a unidirectional compression machine to measure the homogeneous elastic moduli E_1^{hom} and E_3^{hom} . The unidirectional rubber fibers are assembled and lightly stucked together to maintain the arrangement during the test and to assure the straightness of the fibers (Fig. 5). The dimensions of the samples and the compression speed are reported in Table 2.

Fig. 6 shows a curve of the compression of the hexagonal arrangement sample according to the Ox_3 compression direction. In this figure, a short bold curve is the quasi linear part that is selected to calculate the Biot coefficient (stress range between 0.35 MPa and 0.55 MPa), all moduli and coefficients will be determined within this interval.

Table 1
Test types and corresponding moduli.

UD compression	E_3^{hom}, E_1^{hom}	ν_{21}^{hom}
Shear	ν_{31}^{hom}	ν_{21}^{hom}
Drained isotropic compression	k^{hom}	ν_{21}^{hom}
Undrained isotropic compression	k_f	

Table 2
Samples geometry and test conditions.

Tests	UD compression	Isotropic compression	Shear
Diameter	50 mm	50 mm	50 mm
Height	50 mm	100 mm	50 mm
Compression speed	0.2 mm/min	6 kPa/min	0.1 mm/min

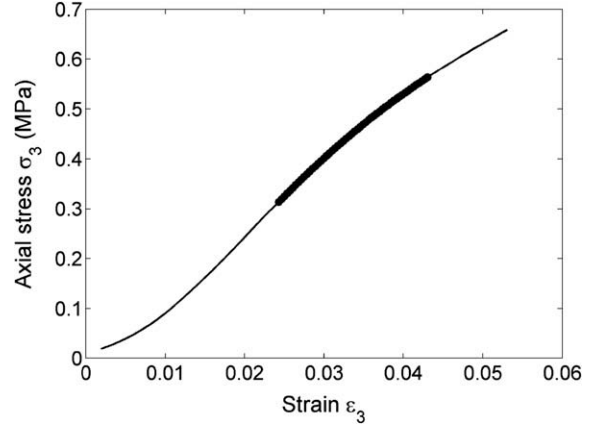


Fig. 6. Response of the hexagonal arrangement under UD compression along Ox_3 axis.

Similarly, the UD compression according to the Ox_1 direction of the square and hexagonal arrangements are measured, the samples are shown as in Fig. 7.

The slope of the quasi linear parts of the stress vs. strain curves gives the tangent moduli E_3^{hom} and E_1^{hom} of the square and hexagonal arrangements. The corresponding graphs of the quasi linear region are presented in Figs. 8 and 9.

5.2. Shear tests

The shear test and the isotropic test are realized with a triaxial machine which is originally used for soils. The impregnated sample is confined in a membrane which isolate it from the confinement water (Fig. 10). The shear test allows to measure two parameters: the elastic modulus (E_3^{hom} and E_1^{hom}) and the Poisson ratio ν_{31}^{hom} . During the test, the displacement of the piston (strain ϵ_3 or ϵ_1), the axial effort (stress σ_3 or σ_1) and the water volume ejected or brought in the cell (volumetric strain ϵ_V) are measured. Starting from these data, the elastic moduli E_3^{hom} and E_1^{hom} are determined. In the infinitesimal deformation, we have

$$\epsilon_V = \epsilon_1 + \epsilon_2 + \epsilon_3 \quad (21)$$



Fig. 7. Square (left) and hexagonal (right) arrangements for compressions along the Ox_1 axis.

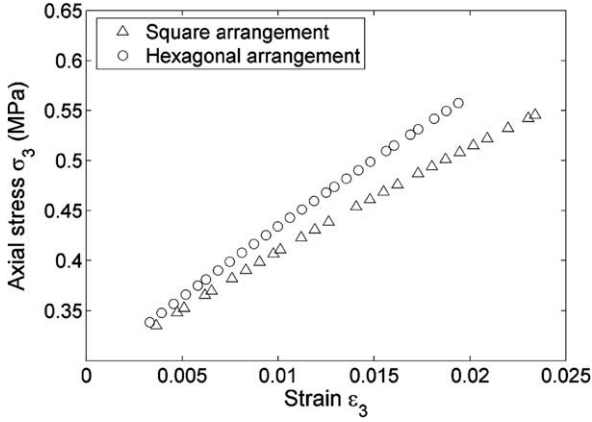


Fig. 8. Stress vs. strain curves of the Ox_3 compression direction in the selected range [0.35 MPa; 0.55 MPa].

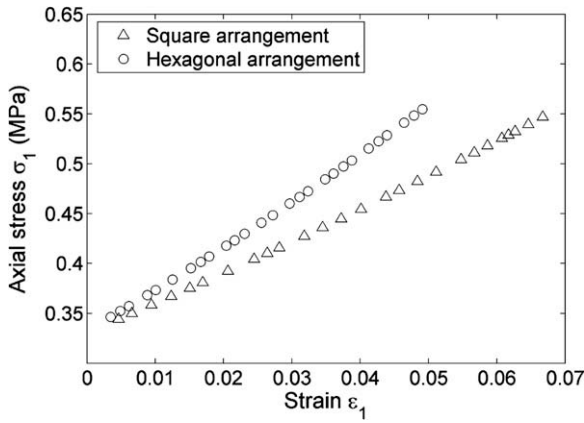


Fig. 9. Stress vs. strain curves of the Ox_1 compression direction in the selected range [0.35 MPa; 0.55 MPa].

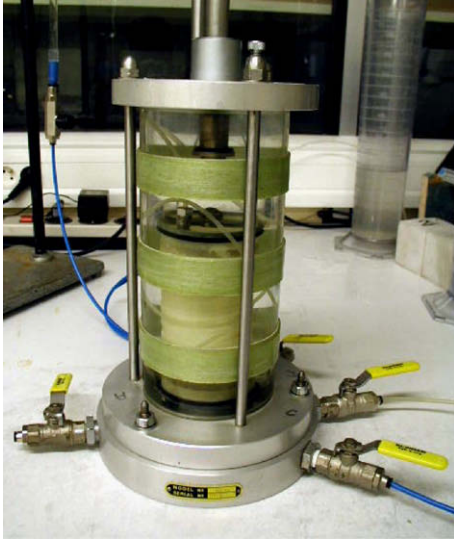


Fig. 10. The cell of the triaxial machine.

Moreover, for the shear test in the Ox_3 direction, $\varepsilon_1 = \varepsilon_2$, which leads to

$$\varepsilon_1 = \frac{\varepsilon_V - \varepsilon_3}{2} \iff v_{31}^{hom} = \frac{\varepsilon_1}{\varepsilon_3} = \frac{\varepsilon_V}{2\varepsilon_3} - \frac{1}{2} \quad (22)$$

where the values of the volumetric strain ε_V and the strain according to the Ox_3 direction ε_3 are given by the shear test.

The curves of the stress vs. strain relations are plotted and show similar trends to the ones in Figs. 6, 8 and 9. The mean values of the Young moduli E_3^{hom} and E_1^{hom} of the two tests are given in Table 3.

The Poisson ratios v_{31}^{hom} for the square and hexagonal arrangements are determined with Eq. (22), the curves of v_{31}^{hom} are presented in Fig. 11 for the chosen stress interval.

The Poisson ratio v_{21}^{hom} cannot be determined directly by shear test. It is determined using the drained bulk modulus k_{hom} , which is measured by an isotropic compression test.

5.3. Isotropic compression tests

The isotropic compression test is also realized with a triaxial machine. The sample is prepared and confined as in the shear test, the amount of confinement water which enters or leaves the cell as function of the isotropic confinement pressure is considered as the deformation of the rubber sample (for drained test) or the deformation of the fiber rubber itself (undrained test). The drained homogeneous bulk modulus k_{hom} is calculated as the ratio of the isotropic confinement compression σ_{iso} to the volumetric strain ε_V of the drained test, whereas the undrained bulk modulus k_f (or the fiber bulk modulus) is calculated from the undrained test. The $\sigma_{iso} - \varepsilon_V$ relations of the drained and undrained tests are given in Figs. 12 and 13.

Theoretically, the two curves in Fig. 13 should coincide because they present the bulk modulus of the rubber. Thanks to the moduli k_{hom} , E_3^{hom} , E_1^{hom} and the Poisson ratio v_{31}^{hom} , the Poisson ratio v_{21}^{hom} is determined by the relation for the transversely isotropic material

$$v_{21}^{hom} = 1 - \frac{E_1^{hom}}{2} \left[\frac{1}{k_{hom}} - \frac{1}{E_3^{hom}} (1 - 4v_{31}^{hom}) \right] \quad (23)$$

After calculation, the values of v_{21}^{hom} are presented in Fig. 14.

The Poisson ratio v_{21}^{hom} is greater than 0.5, it is due to the structure of the sample and not to the behavior of the rubber material, which has a Poisson ratio slightly lower than 0.5 (Poisson ratios exceeding 0.5 may result from anisotropic materials [15]).

5.4. Results of Biot coefficients realized by tests

The Biot coefficients for the transversely isotropic material are determined as function of the five parameters (Eqs. (8) and (9)). Those parameters are reported in Table 3 (the underlined values are the chosen ones).

The Biot coefficients of the square and hexagonal arrangements are presented in Fig. 15.

Firstly, the graph shows that the Biot coefficients are clearly lower than one. This shows that the Terzaghi's hypothesis (Biot coefficient is equal to one) may not be applied for all cases of saturated fibrous materials.

Then, for the same arrangement, the Biot coefficients b_1 according to the weakest resistance direction Ox_1 are always superior to b_3 according to the strongest resistance direction Ox_3 . This shows the influence of the material structure on the Biot coefficients.

Finally, for the same direction of two different structures, the Biot coefficients of the square arrangement are always superior to that of the hexagonal arrangement, thus the Biot coefficients are close to one when the porosity is high. Moreover, the Biot coefficients decrease when the applied stress is raised. Those trends are similar to the ones of Bemer et al. [1] and Ozanam et al. [17], who performed tests for isotropic materials.

Table 3
Summary of the main moduli and Poisson ratios obtained from the tests.

Tests	Parameters						
	E_3^{hom} (MPa)		E_1^{hom} (MPa)		ν_{31}^{hom}	ν_{21}^{hom}	k_f (MPa)
	UD compr.	Shear	UD compr.	Shear	Shear	Shear isotropic compr.	Isotropic compr.
Square	12.7	13.8	3.2	3.3	0.484	0.713	72.3
Hexagonal	15.7	13.6	4.4	4.6	0.484	0.697	63.5

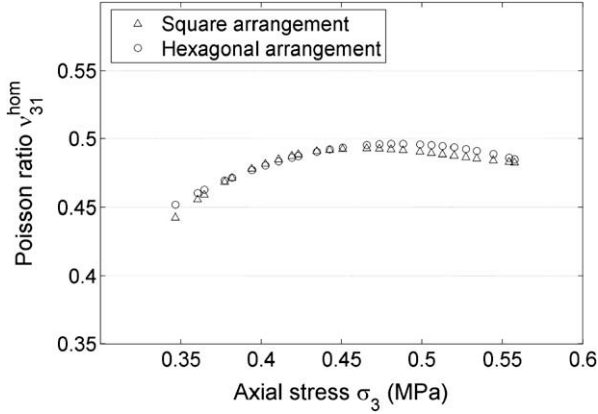


Fig. 11. Poisson ratio ν_{31}^{hom} for square and hexagonal arrangements.

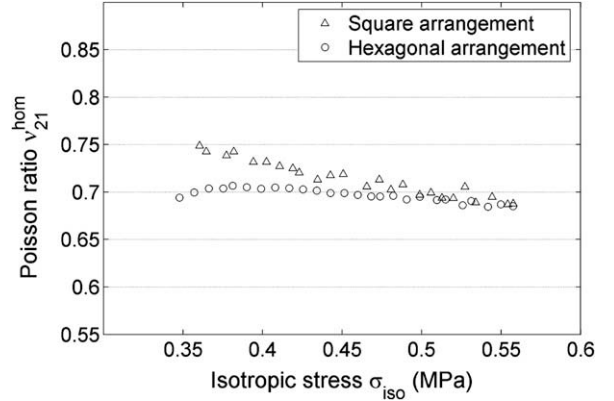


Fig. 14. Poisson ratio ν_{21}^{hom} for square and hexagonal arrangements.

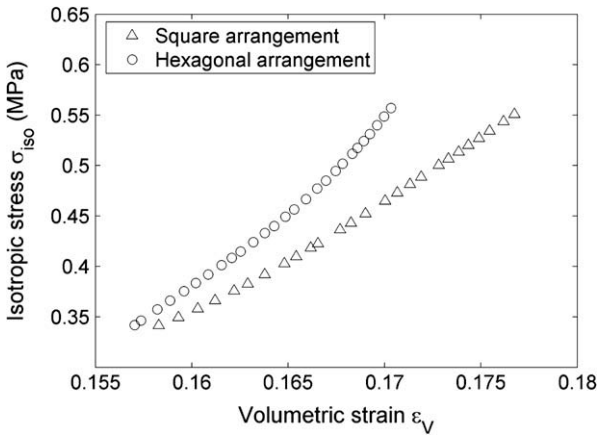


Fig. 12. Isotropic stress vs. volumetric strain for square and hexagonal arrangements in drained conditions.

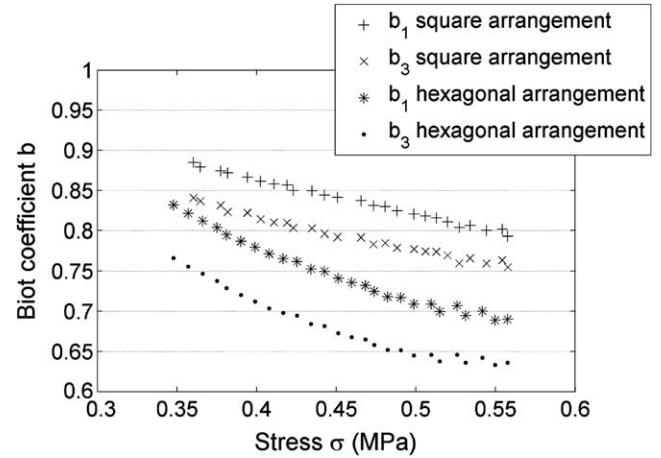


Fig. 15. Biot coefficients of the square and hexagonal arrangements.

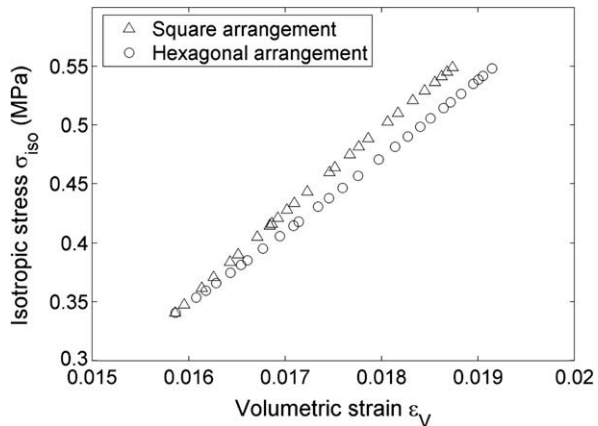


Fig. 13. Isotropic stress vs. volumetric strain for square and hexagonal arrangements in undrained conditions.

6. Theoretical and experimental comparison

The experimental mean values of the Biot coefficients for the square and hexagonal arrangements (Table 4) are presented in Fig. 16 as function of the initial porosity with the theoretical curves of the Mori–Tanaka and Ponte Castañeda–Willis schemes.

These curves are drawn with the Poisson ratio of the rubber fiber $\nu = 0.48$. This value is determined from tensile tests of the rubber fiber combined with a digital camera. The pictures taken during the tests show the variation of the radial and longitudinal strains, from which the Poisson ratio is determined.

Table 4
Experimental mean values of the Biot coefficients.

	b_1	b_3	Initial porosity
Square	0.837	0.793	0.215
Hexagonal	0.746	0.682	0.093

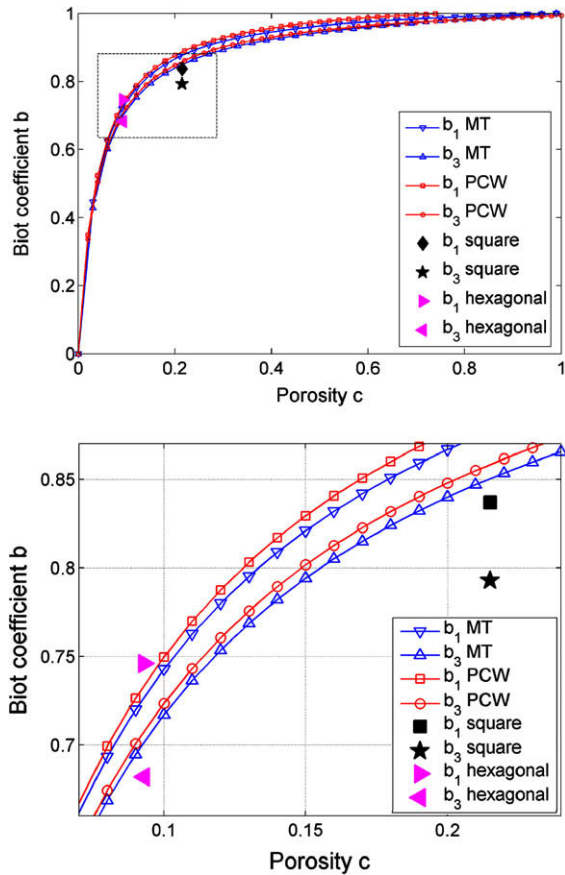


Fig. 16. Theoretical and experimental results of the Biot coefficients, with $\nu = 0.48$.

We find a rather good agreement between the theoretical and experimental results. In fact, the four experimental points in Fig. 16 should move a bit towards the left because these points are plotted as function of the initial porosity, whereas during the tests, the porosity of the fiber material is slightly reduced.

7. Conclusion

Experimental Biot coefficients for unidirectional fiber assemblies have been obtained following a procedure that involved uniaxial and triaxial testing machines. Micromechanical schemes have also been used and combined to the poromechanical theory in order to obtain Biot coefficients of unidirectional fiber assemblies. Both micromechanical and experimental results are in good agreement. For the fiber assemblies studied in this article, the Mori-Tanaka scheme seems to be a good choice to estimate the homogeneous stiffness tensor.

The theoretical results are based on the assumptions of isotropy and perfect straightness of the fibers. That first result is somehow limited to some applications, but it is a starting point for former

evolutions towards the reality of composites manufacturing. It suggests that the Biot coefficients of a UD assembly of isotropic fibers is lower than one and that Terzaghi's assumption is not valid for this specific case. Improvements should take into account specificities such as the transverse isotropy of fibers, and localized contacts, finite and non-linear deformations of fiber assemblies. In the case of localized contacts between fibers, more complex distributions are needed and the Ponte Castañeda-Willis scheme would be preferred.

References

- [1] Bemer E, Longuemare P, Vincké O. Poroelastic parameters of Meuse/Haute Marne argillites: effect of loading and saturation states. *Appl Clay Sci* 2004;26:359–66.
- [2] Benveniste Y, Dvorak GJ, Chen T. On diagonal and elastic symmetry of the approximate effective stiffness tensor of heterogeneous media. *J Mech Phys Solids* 1991;39:927–46.
- [3] Bismarck A, Mishra S, Lampke T. Chapter 2: plant fibers as reinforcement for green-composites. In: Mohanty AK, Misra M, Drzal LT, editors. *Natural fibers biopolymers, and biocomposites*. CRC Press; 2005. p. 37–108.
- [4] Bornert M, Bretheau T, Gilormini P. *Homogenization in mechanics of materials*. ISTE Publishing Company; 2006.
- [5] Chateau X. Méthode d'estimation pour l'homogénéisation des matériaux élastiques linéaires. In: *Approches multiéchelles pour les matériaux et les structures du génie civil*. Actes des journées scientifiques du LCPL, Nantes, France, June 2000.
- [6] Coussy O. *Poromechanics*. John Wiley & Sons; 2004.
- [7] Dormieux L, Kondo D, Ulm FJ. *Microporomechanics*. John Wiley & Sons Inc.; 2006.
- [8] Eshelby JD. The determination of the elastic field of an ellipsoidal inclusion, and related problems. *Proc Roy Soc London A* 1957;241:376–96.
- [9] Federico S, Grillo A, Herzog W. A transversely isotropic composite with a statistical distribution of spheroidal inclusions: a geometrical approach to overall properties. *J Mech Phys Solids* 2004;52:2309–27.
- [10] Giraud A, Huynh QV, Hoxha D, Kondo D. Application of results of Eshelby tensor to the determination of effective poroelastic properties of anisotropic rocks-like composites. *Int J Solids Struct* 2007;44:3756–72.
- [11] Giraud A, Huynh QV, Hoxha D, Kondo D. Effective poroelastic properties of transversely isotropic rocks-like composites with arbitrarily oriented ellipsoidal inclusions. *Mech Mater* 2007;39:1006–24.
- [12] Gutowski TG, Morigaki T, Cai Z. The consolidation of laminate composites. *J Compos Mater* 1987;21:172–88.
- [13] Han K, Lee LJ, Liou M. Fiber mat deformation in liquid composite molding. *Polym Compos* 1993;14:151–60.
- [14] Hill R. Theory of mechanical properties of fiber-strengthened materials: I. Elastic behaviour. *J Mech Phys Solids* 1964;12:199–212.
- [15] Lee T, Lakes RS. Anisotropic polyurethane foam with Poissons ratio greater than 1. *J Mater Sci* 1997;32:2397–401.
- [16] Mura T. *Micromechanics of defects in solids*. Springer; 1987.
- [17] Ozanam O, Hoteit N, Bemer E, Heitz JF. Experimental determination of poroelastic parameters of a clayey rock. In: Auriault JL et al., editors. *Second Biot conference on poromechanics*. Grenoble, France, 26–28 August 2002. Zwets & Zeitlinger, Lisse, Netherlands. p. 275–80.
- [18] Ponte Castañeda P, Willis JR. The effect of spatial distribution on the effective behavior of composite materials and cracked media. *J Mech Phys Solids* 1995;43:1919–51.
- [19] Ray D, Rout J. Chapter 9: thermoset biocomposites. In: Mohanty AK, Misra M, Drzal LT, editors. *Natural fibers biopolymers and biocomposites*. CRC Press; 2005. p. 291–347.
- [20] Saunders RA, Lekakou C, Bader MG. Compression in the processing of polymer composites: 2. Modelling of the viscoelastic compression of resin-impregnated fiber networks. *Compos Sci Technol* 1999;59:1483–94.
- [21] Suvorov AP, Dvorak GJ. Rate form of the Eshelby and Hill tensors. *Int J Solids Struct* 2002;39:5659–78.
- [22] Walpole LJ. Fourth-rank tensors of the thirty-two crystal classes: multiplication tables. *Proc Roy Soc London A* 1984;391:149–79.